Available online at **www.joac.info**

ISSN: 2278-1862

Journal of Applicable Chemistry

2018, 7 (3): 501-512

(International Peer Reviewed Journal)

Synthesis, Thermo-Optical Characterization, Crystal Structure, Hirshfeld Surface Analysis and DFT Studies Of ((4-Chloro-6-Methyl-2-Oxo-2H-Chromen-3-Yl) Methylene) Benzene-Sulfonohydrazide

K.N. Chethan Prathap[1, 2], S.R. Kumara Swamy[3], M. Prabhuswamy[4], Ismail Warad [5] and N.K. Lokanath[1]*

1. Department of Studies in Physics, Manasagangotri, University of Mysore, Mysuru 570 006, **INDIA**
2. Department of Physics, University College of Science, Tumkur University, Tumakuru 572 102, **INDIA**
3. Department of Physics, Maharani's Science College for Women, Mysuru 570 005, **INDIA**
4. Department of Physical Science Education, JSS Institute of Education, Sakaleshpur 573 134, **INDIA**
5. Department of Chemistry, Science College, An-Najah National University, Nablus, **PALESTINE**

E-mail: lokanath@physics.uni-mysore.ac.in

Accepted on 18th April, 2018

ABSTRACT

The coumarin derivative ((4-chloro-6-methyl-2-oxo-2H-chromen-3-yl) methylene) benzene-sulfono-hydrazide was synthesized by condensation reaction, characterized by spectroscopic techniques (^{1}H NMR, ^{13}C NMR, FTIR, UV-Vis, TGA and DSC) and finally the structure was confirmed by X-ray diffraction method. The thermal studies showed that the title compound is thermally stable up to 200°C and they undergo endothermic decomposition at higher temperatures. The crystal structure revealed that the compound crystallizes in $P\bar{1}$ space group. The compound exhibits diverse intermolecular interactions including C-H…O, N-H…O, C-H…Cl type of hydrogen bonds, C-Cl…Cg and Cg…Cg interactions. The molecules form alternative $R_2^2(14)$ and $R_4^4(20)$ supramolecular synthons through intermolecular hydrogen bonds which connect them to an infinite one-dimensional chain along [0 11] direction. The Hirshfeld surface analysis showed that H…H (29.4%) and O…H (28.7%) are the major intermolecular interactions. Further the structure was optimized using density functional theory (DFT) calculations. The optimized geometrical parameters show very good agreement with those determined by XRD method. The time dependent density functional theory (TDDFT) calculation was used to study electronic transition among the first 15 molecular orbitals. The calculated electronic absorption spectrum compliments the experimentally measured UV-Vis spectrum.

Graphical Abstract

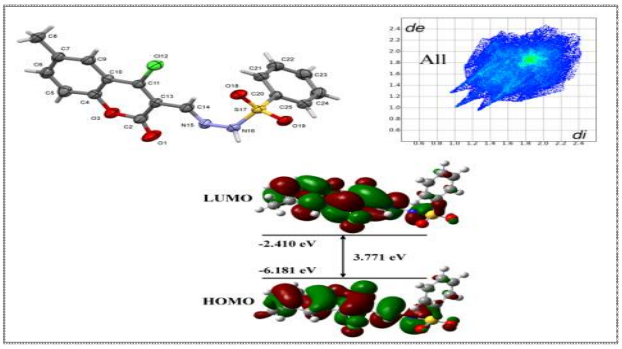

Keywords: Coumarin-sulfonylhydrazide, Crystal Structure, UV-Visible, Density Functional Theory.

INTRODUCTION

Coumarins belong to important class of oxygen containing fused heterocyclic compounds. Since their isolation from Tonka bean in 1820, they have been used extensively in perfumes, fabric conditioners and more importantly in pharmaceuticals. Coumarin derivatives form an elite class of compounds with diverse therapeutic activities such as antioxidant, anti-inflammatory, antitumor, antiviral, antituberculosis and antimicrobial [**1-6**]. Coumarin, biscoumarin and furanocoumarin derivatives have been reported as potential inhibitors of HIV-1 replication with anti-HIV activity [**7-10**]. Synthetic and natural coumarin derivatives as cytotoxic agents have been studied for their anticancer and antitumor activities [**11-15**]. Studies have been carried out on coumarin derivatives as potential seed protectants, pesticides and rodenticides [**16-18**]. Coumarin derivatives have been demonstrated with anion sensing chemo-receptors [**19-21**]. Metal complexes of coumarin derivatives have been reported as effective fluorescent properties suitable for applications in living cells [**22-24**].

Motivated by the diverse biological importance of the coumarin derivatives, we synthesized novel coumarin derivative ((4-chloro-6-methyl-2-oxo-2H-chromen-3-yl)methylene) benzene-sulfono-hydrazide, characterized by various spectroscopic techniques. The thermal properties were investigated by thermogravimetric analysis (TGA) and differential scanning calorimetry (DSC). The electronic absorption was studied using UV-Vis spectrum and theoretically calculated spectrum using time dependent density functional theory (TDDFT) calculations. Finally, the structure was confirmed by X-ray diffraction method. Further, the structural optimization was carried out using density functional theory (DFT) calculations. The structural parameters determined using X-ray diffraction method was compared with the theoretically optimized parameters. Frontier molecular orbitals (HOMO-LUMO), global and local indices, electronic absorption spectrum were also studied using DFT calculations.

MATERIALS AND METHODS

The chemicals used in the synthesis of the title compound were purchased from Sigma-Aldrich co., and were used without any further purification. TLC was used to monitor the progress of the reaction, was carried out with precoated aluminum-backed plate (Merck Silica Gel 60 F_{254}) and visualized under UV light (λ=256 nm). Melting point was determined using Chemocline melting point apparatus CL725. NMR spectra (^{1}H and ^{13}C) were recorded on a Bruker Avance spectrometer and chemical shifts (δ) are reported in parts per million (ppm) relative to TMS. The FTIR characterization was carried out on a Perkin Elmer 100 FT-IR spectrometer (ν are in cm^{-1}). Thermal analysis was performed using a Perkin Elmer DSC 8000 and Pyris 1 TGA systems. UV-Vis spectrum was recorded with Perkin Elmer Lambda 35 spectrometer between 250 nm to 700 nm.

Synthesis of ((4-chloro-6-methyl-2-oxo-2H-chromen-3-yl)methylene)benzenesulfono-hydrazide: The title compound (**3**) was synthesized using 5 mmol of 4-chloro-3-formyl-6-methylcoumarin (**1**) and 5 mmol of benzene sulfonohydrazide (**2**) in 20 mL of absolute ethanol by nucleophilic addition followed by dehydration. The reaction mixture was refluxed at 78°C for 6 h and the product formation was confirmed by TLC on silica gel precoated aluminum plates with ethyl acetate and hexane (1:5) as eluting solvent. The precipitated compound was filtered, washed with ice cold ethanol and dried at reduced pressure (yield: 91%, melting point: 214-216°C). The crude compound was further purified and crystallized with a mixture of acetone and methanol (2:1) which resulted light yellow color crystals of the compound. The schematic representation of the reaction is shown in figure 1.

Spectroscopic analysis: ^{1}H NMR (DMSO-d6, 300 MHz): δ 7.96 (s, 3H), δ 7.76 (d, 2H), δ 7.68 (d, 1H), δ 7.63 (d, 1H), δ 7.55 (d, 2H), δ 7.36 (dd, 2H), δ 2.38 (s, 3H) ppm; ^{13}C NMR (DMSO-d6, 100

MHz): 168.3, 157.5, 145.2, 137.1, 134.6, 133.8, 132.9, 130.9, 128.3, 126.7, 112.3, 20.8 ppm; FTIR ν/cm^{-1}: 3238, 3174, 3125, 1693, 1605.

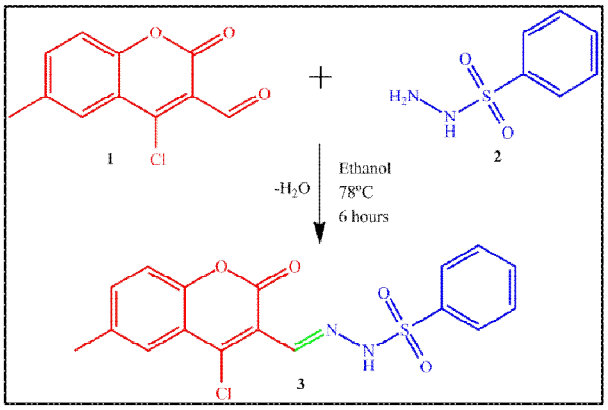

Figure 1. Schematic representation of the reaction pathway of the title compound.

The FT-IR peak at 3238 cm^{-1} corresponds to N-H stretching vibration, multiple peaks in the range of 3125-3174 cm^{-1} corresponds to multiple vibrations of Ar-H protons. The stretching vibration of C=O of the coumarin ring results in a peak at 1693 cm^{-1}. The peak at 1605 corresponds to azomethine bond (C=N) stretching.

Table 1. Crystal structure and refinement details.

Parameter	Value	Parameter	Value
Empirical formula	$C_{17}H_{13}ClN_2O_4S$	μ (mm^{-1})	0.396
Formula weight	376.8	F_{000}	388
Temperature (K)	293(2)	Crystal size (mm^3)	0.24 × 0.35 × 0.30
Radiation	MoKα	2θ range for data collection (°)	6.914 to 55.012
Wavelength(Å)	0.71073	Index ranges	-10 ≤ h ≤ 10; -12 ≤ k ≤ 13; -10 ≤ l ≤ 14
Crystal system	Triclinic	Reflections collected	4644
Space group	$P\bar{1}$	Independent reflections	3577
a (Å)	8.196(4)	Absorption correction	Multi scan
b (Å)	10.385(7)	Refinement method	Full matrix least-squares on F^2
c (Å)	11.242(7)	Parameters	227
α (°)	110.54(5)	Goodness-of-fit on F^2	0.997
β (°)	109.59(7)	Final R indexes [I>=2σ (I)]	R_1 = 0.0554, wR_2 = 0.1465
γ (°)	99.44(4)	Final R indexes [all data]	R_1 = 0.0715, wR_2 = 0.1638
Volume (Å^3)	800.0(8)	Largest diff. peak/hole (eÅ^{-3})	0.46/-0.56
Z	2	CCDC deposit No.	1559677
ρ_{calc}(Mg m^{-3})	1.564		

X-ray diffraction studies: Block shaped single crystal of dimension 0.24 × 0.35 × 0.30 mm^3 was used for X-ray diffraction study. X-ray intensity data were collected at 293 K on a Rigaku XtaLAB mini diffractometer using MoKα radiation of wavelength 0.71073 Å. The data were collected for different settings of φ (0° to 90°), with scan width of 0.5°, exposure time of 3 s and the sample to detector distance of 50 mm. The complete data set was processed using crystal clear [25]. The experimental analysis revealed that the title compound crystallizes in triclinic crystal system with $P\bar{1}$ space group. The crystal structure was solved by direct methods and refined by full-matrix least

squares on F^2 using SHELXS and SHELXL programs respectively [26-27]. All the non-hydrogen atoms were revealed in the first difference Fourier map itself. The hydrogen atoms were positioned geometrically and refined using a riding model with $U_{iso}(H)=1.2\ U_{eq}(C)$ for aromatic (C–H = 0.93 Å) and $U_{iso}(H)=1.5\ U_{eq}(C)$ for $–CH_3$(C–H = 0.97 Å). After several cycles of refinement, the peaks in the difference Fourier map showed no chemical significance and residual was saturated to 0.0554. The details of the crystal structure and data refinement are given in table 1. All the geometrical calculations were carried out using the program PLATON [28] and the diagrams were generated using the software MERCURY [29].

Hirshfeld surface analysis: Hirshfeld surface analysis is one of the most useful tools for exploring different intermolecular interactions and packing modes in crystals. Hirshfeld surface characteristics provide a visual picture of intermolecular interactions, molecular shapes in the crystalline environment in a very subtle way. Analysis of the d_{norm} and shape index mapped Hirshfeld surfaces were carried out and finger print plots were generated using the software Crystal Explorer version 3.0 [30-32]. Surface features that are characteristic of different intermolecular interactions can be identified and these features can be visualized by color coding interior (d_i) or exterior (d_e) distances of the surface to the atoms. The d_{norm} mapped on the Hirshfeld surfaces were generated with color scale in between -0.144 au (blue) to 1.38 au (red) respectively. The 2D fingerprint plots were displayed with d_e and d_i distance in the range of 0.4-2.6 Å. Further the shape index mapped Hirshfeld surfaces were used to visualize different types of interactions [33-35].

Density functional theory calculations: The geometrical structure optimization of the title compound was carried out in gas phase by density functional theory (DFT) calculations using B3LYP functionals with 6-311+G(d,p) level basis set [36-38]. The electronic absorption spectrum was calculated by studying the transitions among different molecular orbitals using time dependent density functional theory (TD-DFT) at the same level of the theory for transitions involving both singlet and triplet states [39]. The Mulliken charges, frontier molecular orbitals, energy gap were calculated. Local and global indices such as electronegativity, chemical potential, hardness, softness and electrophilicity were estimated using Koopman's approximation [40]. The molecular electrostatic potential (MEP) maps were plotted to visualize the possible reactive sites. All the above calculations were performed using Gaussian 09 package [41] and were visualized using GaussView without any constraints on the geometry [42].

RESULT AND DISCUSSION

Optical absorption studies: Optical properties of the title molecule were investigated using UV-Vis spectroscopy. The solution of the title compound in DMSO with a concentration of 25 μgmL^{-1} was used to measure UV-Visible absorbance in the range of 250 nm to 700 nm. The compound showed no absorbance for wavelengths more than 550 nm below which it exhibited significant absorbance. The spectrum exhibits two absorption bands with peaks at 312 nm and 467 nm. The experimentally measured UV-Vis absorbance spectrum is shown in figure 2 using red curve.

Thermal analysis: The thermal properties of the title molecule were studied using differential scanning calorimetry (DSC) and thermogravimetric analysis (TGA). The DSC was carried out using 4.0 mg of the title compound in an aluminum sample pan with a heating rate of 10°C min^{-1} in dynamic nitrogen atmosphere (15 mL min^{-1}). The TG analysis was performed using 7.6 mg of title compound in a platinum crucible which is heated at a rate of 10°C min^{-1} in dynamic nitrogen atmosphere with 15 mL min^{-1} flow rates. Figure 3 show the DSC and TGA responses of the title compound. The title compound exhibits two endothermic peaks in DSC curve at 218°C and 22°C respectively. The first peak corresponds to the melting and the second peak may be associated with endothermic decomposition of the compound.

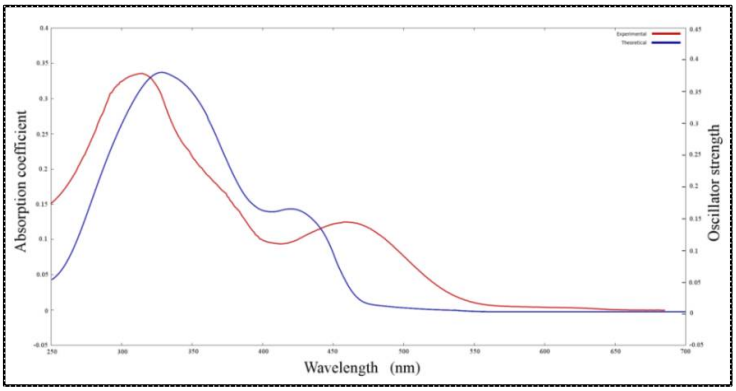

Figure 2. Experimental (red) and calculated (blue) UV-Vis spectrum of the title compound.

The TGA curve shows no drop in the mass of the compound till 200°C which indicates that the compound is thermally stable up to a temperature of 200°C. The mass of the sample used for TGA experiment shows a sudden decrease after 200°C. The decrease in mass was observed at a high rate from 200°C to 250°C with a mean temperature of 225°C. This decrease in the mass is associated with the decomposition of the title compound. The position of the second peak in the DSC curve and the mean temperature of this decrease are in very good correlation and complement each other. About 57% decrease in the mass was observed between 200°C and 350°C. A second drop in the mass was observed between 400°C to 500°C. This second weight loss corresponds to the evaporation of volatile fragments leaving behind very small amount of (<1%) of carbon char.

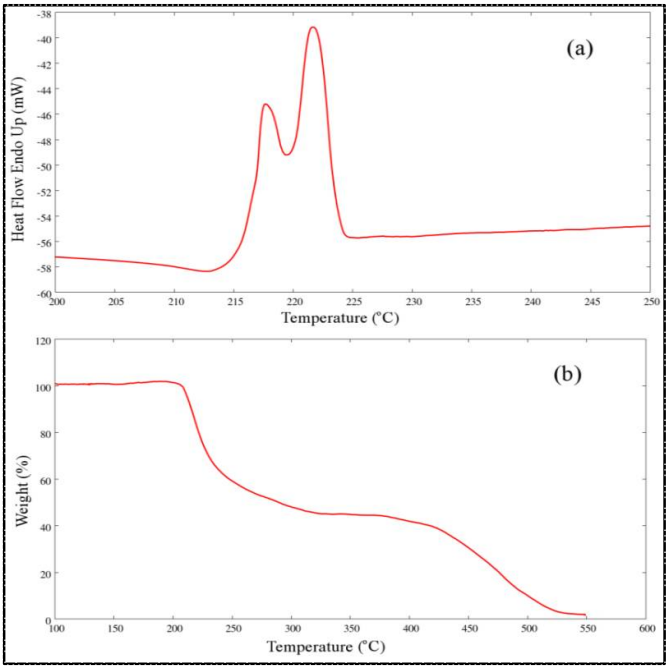

Figure 3. (a) DSC and (b) TGA responses of the title compound.

X-ray diffraction studies: The molecular structure of the title compound consists of 11 atom membered coumarin moiety substituted with chlorine atom and a methyl group at position 4 and 7 respectively and a benzene ring connected to the coumarin moiety through a sulfonohydrazide moiety at position 3. The coumarin moiety is planar with a dihedral angle of 2.11(4) ° between the fused benzene and pyran rings. The dihedral angle between the coumarin and benzene ring that is attached

through sulfonylhydrazide moiety is 86.72(1) °. A torsion angle of 176.7(3) ° indicates that the title compound is in *E*-conformation with respect to the C=N bond. Figure 4 represents the ORTEP of the title compound with thermal ellipsoids drawn at 50% probability. The structural parameters such as bond length and bond angles are in very good agreement with the similar structures. Table 2 lists selected bond lengths, bond angles and torsion angles of the title compound.

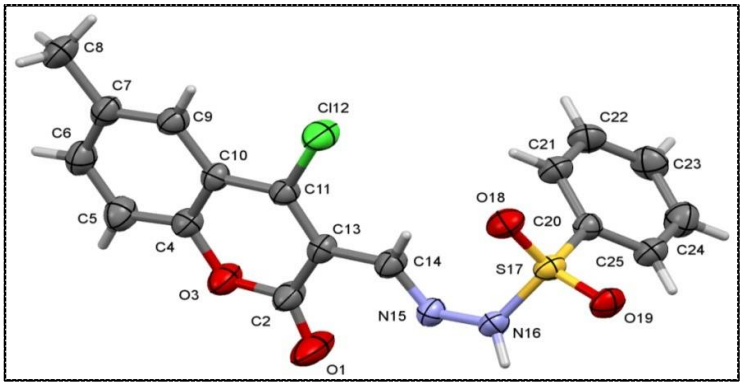

Figure 4. ORTEP of the title compound with thermal ellipsoids drawn at 50% probability.

The crystal and molecular structure of the title compound is stabilized by various intermolecular interactions. The compound exhibits two C—H…Cl and a C—H…O type of intra molecular hydrogen bonds which accounts for the stability of the molecular structure. Also, the title compound exhibits N—H…O and C—H…O type of intermolecular hydrogen bonds which form alternative $R_2^2(14)$ and $R_4^4(20)$supramolecularsynthons connecting the molecules into a one- dimensional infinite chain along [011] direction as shown in figure 4. The details of the hydrogen bond geometry are listed in table 3. The presence of chlorine atom which has the highest electron affinity among all the elements, contribute significantly to the crystal structure stability by exhibiting C11–Cl12…Cg1 and C11–Cl12…Cg3 (Cg1 and Cg3 are center of gravity of pyran and terminal benzene rings respectively) interactions. Further the coumarin rings are stacked with two Cg–Cg interactions between the fused benzene rings and pyran rings of adjacent molecules as shown in figure 4. Different interaction details are listed in the table 4. The results were compared with previously reported molecules with similar structure and found to be in very good agreement [**43**].

Table 2. Selected bond lengths, bond angles and torsion angles of the title compound.

Selected bond lengths (Å)			Selected bond angles (°)			Selected torsion angles (°)		
	XRD	DFT		XRD	DFT		XRD	DFT
O1-C2	1.193(5)	1.203	O1-C2-O3	115.7(3)	116.82	C14-N15-N16-S17	36.6(4)	30.00
O3-C2	1.373(4)	1.393	O3-C2-C13	118.0(3)	116.57	N15-N16-S17-O18	54.5(3)	57.94
O3-C4	1.371(4)	1.359	O18-S17-O19	119.38(3)	122.97	N15-N16-S17-C20	61.9(2)	57.35
N15-C14	1.275(4)	1.288	O18-S17-N16	108.6(2)	107.62	O3-C2-C13-C11	3.8(4)	2.41
Cl12-C11	1.728(2)	1.757	N16-S17-C20	105.76(1)	105.91	C2-C13-C14-N15	10.5(5)	18.03
S17-N16	1.659(2)	1.728	N16-N15-C14	118.5(2)	120.51	C13-C14-N15-N16	176.7(3)	178.65
N15-N16	1.393(3)	1.363	S17-N16-N15	125.47(9)	128.47	C21-C20-S17-N16	96.0(2)	98.18
C4-C10	1.392(4)	1.405	S17-C20-C25	118.8(2)	118.70	C25-C20-S17-N16	85.0(2)	81.50
C13-C14	1.460(5)	1.463	N15-C14-C13	122.7(3)	121.18	S17-C20-C25-C24	179.4(2)	179.08
S17-C20	1.760(3)	1.795	Cl12-C11-C10	117.3(2)	116.79	C25-C20-S17-O19	27.1(2)	28.12
Correlation coefficient: 0.99344			Correlation coefficient: 0.94817			Correlation coefficient: 0.99946		

Hirshfeld surface analysis: Hirshfeld surface analysis was carried out with d_{norm}/shape index mapped Hirshfeld surfaces and finger print plots to visualize and understand the intermolecular interactions of the title compound. Figure 5(a) shows the d_{norm} mapped Hirshfeld surface where the red spots

represent the high interaction regions. Similarly figure 5(b) and 5(c) depict the shape index mapped Hirshfeld surface highlighting C…C and C…Cl interactions. The H…H and O…H (N—H…O and

Table 3. Different interactions of the title compound.

Hydrogen bond								
No.	**Type**	**Donor**	**H**	**Accepter**	**D—H(Å)**	**H…A(Å)**	**D…A(Å)**	**D—H…A(°)**
1	Inter[i]	N(16)	H(16)	O(1)	0.86	2.3	2.905(4)	128
2	Inter[j]	C(5)	H(5)	O(19)	0.93	2.54	3.406(4)	155
3	Intra	C(9)	H(9)	Cl(12)	0.93	2.68	3.066(4)	106
4	Intra	C(14)	H(14)	Cl(12)	0.93	2.58	2.993(4)	107
5	Intra	C(14)	H(14)	O(18)	0.93	2.18	2.919(4)	136
i: *1-x,1-y,1-z*; j: *x,1+y,1+z*								
C—Cl…Cg interaction								
Y—X…Cg			X…Cg (Å)		Y…Cg (Å)		Y--X…Cg(°)	
C11—Cl12…Cg1[i]			3.846(3)		3.471(4)		64.46 (1)	
C11—Cl12…Cg3[j]			3.533(3)		5.214(4)		163.83(1)	
i: *1-x, 2-y, 1-z* ii: *-x, 1-y, -z*								
Cg…Cg interaction								
Cg(I)…Cg(J)	Cg…Cg(Å)	Alpha (°)	Beta (°)	Gamma (°)	CgI_Perp(Å)		CgJ_Prep(Å)	
Cg(1)…Cg(1)[i]	3.766(3)	0	23.6	23.6	3.4507(2)		3.4507(2)	
Cg(2)…Cg(2)[j]	3.951(3)	0	25.6	25.6	-3.5619(3)		-3.5619(3)	
i: *1-x,2-y,1-z*; j: *-x,2-y,1-z*								

C—H…O) interactions are the major contributors to the Hirshfeld surface with contribution of 29.4% and 28.7% respectively. Due to Cg…Cg interactions, the C…H and C…C intermolecular contacts contribute significantly to the Hirshfeld surface with a contribution of 16% and 6.9% respectively. About 5.2% of contribution is from C…Cl intermolecular contacts due to the presence of Cl…Cg interactions. Figure 6 shows the fingerprint plots generated for different intermolecular interactions along with their contribution

Table 4. Calculated energy values, associated global, local indices, total polarizability and total first order static hyperpolarizability of the title molecule.

Parameter	Value
E_{HOMO} (eV)	-6.181
E_{LUMO} (eV)	-2.410
ΔE (eV)	3.771
Electronegativity (χ) (eV)	4.296
Chemical potential (μ) (eV)	-4.296
Global hardness (η) (eV)	1.886
Global softness (s) (eV^{-1})	0.265
Electrophilicity index (ω) (eV)	4.893
Dipole moment (Debye)	6.935
Isotropic polarizability (10^{-24} esu)	37.724
Static hyperpolarizability (10^{-30} esu)	9.613

Density functional theory calculations: The coordinates of the title compound were optimized using density functional theory (DFT) calculations using B3LYP hybrid Becke, three-parameter, Lee-Yang-Parr (B3LYP) functional at 6-311+G(d,p) level of the theory. Selected structural parameters from DFT calculations are compared with those obtained from XRD studies in table 2. The structural parameters from the optimized structure compliment with those determined using XRD studies yields very good correlation coefficient. The direct energy gap between the frontier molecular orbitals (HOMO-LUMO) was found to be 3.771 eV. The global and local indices such as electronegativity (χ), chemical potential (μ), global hardness (η), global softness (s) and electrophilicity index (ω) are estimated and listed in table 4. The molecular electrostatic potential map (MEP) was plotted to identify the possible reactive locations of the title compound (Figure 7). Further, the transitions

among different molecular orbitals were studied using time dependent density functional theory (TDDFT) calculations. The electronic absorption spectrum obtained from TDDFT calculations are shown in figure 2 along with the experimentally determined UV-Vis absorption spectrum.

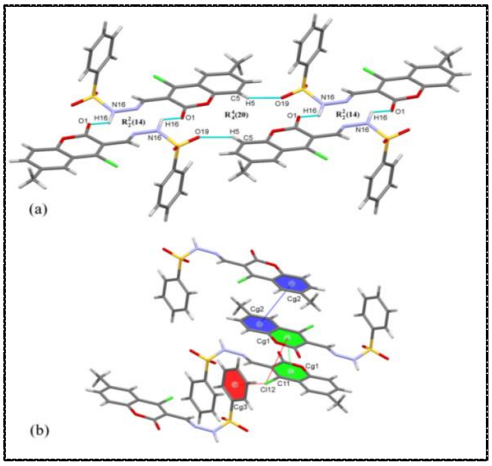

Figure 4. Various interactions of the title compound: (a)hydrogen bond (b) C—Cl…Cg (red) and Cg…Cg (green and blue).

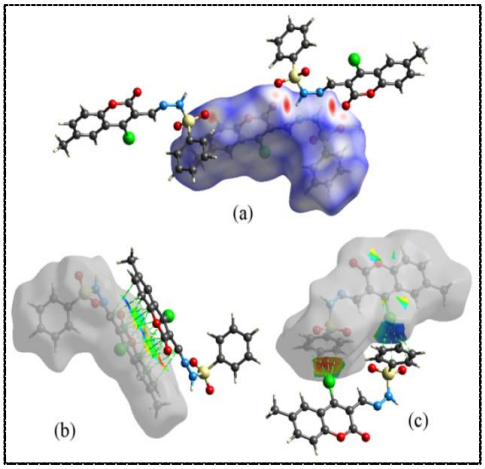

Figure 5. Hirshfeld surfaces mapped with (a) d_{norm} (b) shape index showing C…C interaction (c) shape index highlighting Cl…C interactions of the title compound.

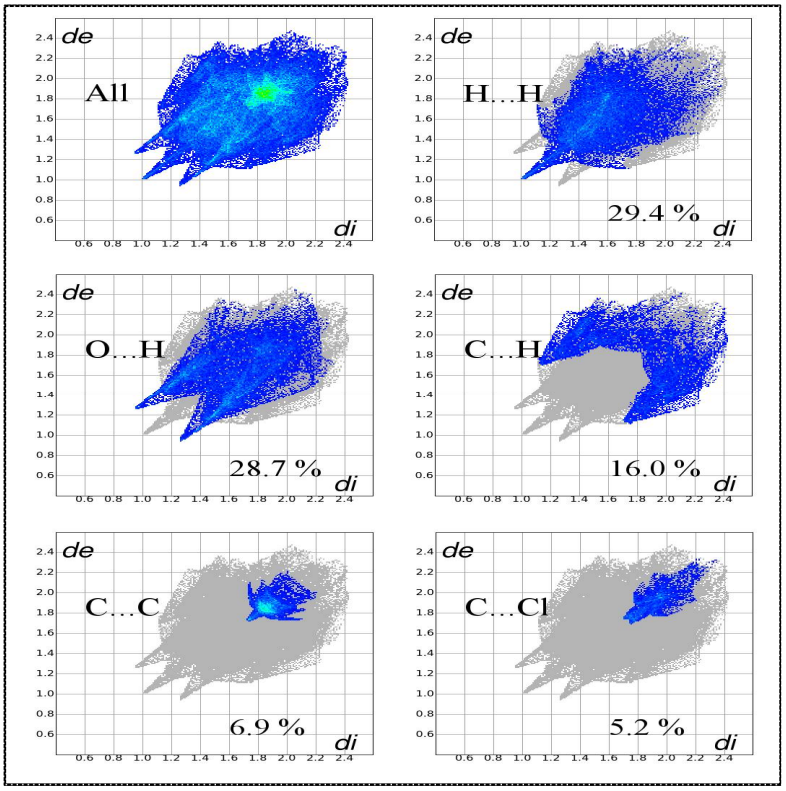

Figure 6. 2D finger print plots showing contribution of different intermolecular interactions of the title compound.

The electronic absorption calculations were carried out for both singlet and triplet state transitions with DMSO solvent environment using IEFPCM model. The highest absorption was observed with respect to the transition between the frontier molecular orbitals (HOMO-LUMO) at 328 nm with

oscillator strength of 0.4434. Another weak but significant peak was observed at 435 nm with oscillator strength of 0.1826. Further the NLO properties of the molecule were investigated by computing first order hyperpolarizabilities which showed that the molecule exhibits significantly large first order static hyperpolarizabilities which is about 20 times larger than the reference material urea.

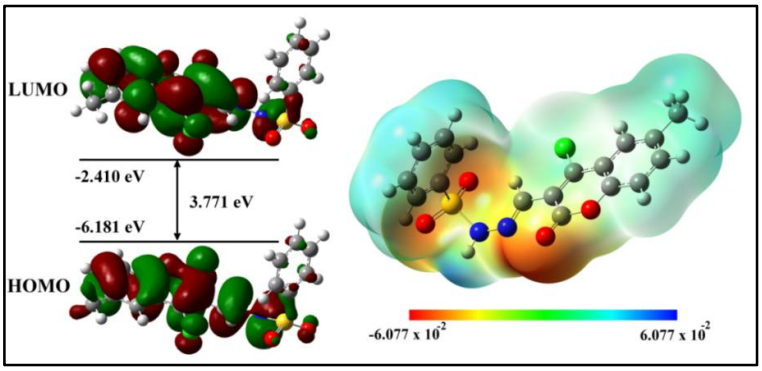

Figure 7. HOMO-LUMO and MEP of the title compound.

APPLICATION

With high thermal stability and no absorbance in the visible region of the spectra indicate that the title compound can be a potential candidate for high energy optical applications. Further, high hyperpolarizability values for the compound make it a promising candidate for NLO applications.

CONCLUSIONS

A novel coumarin derivative containing benzene sulfonohydrazide moiety was synthesized by condensation reaction between. The compound was characterized by various spectroscopic techniques and the structure was confirmed by X-ray diffraction method. The thermal studies demonstrated high thermal stability of the title compound up to 200°C, at higher temperature the compound undergo endothermic decomposition. The optical studies revealed that the compound exhibit no absorption in the visible region but good absorbance in the measured UV region with an absorption peak at 312 nm. The title compound exhibits diverse intermolecular interactions including C—H…O, N—H…O, C—H…Cl type of hydrogen bonds, C—Cl…Cg and Cg…Cg interactions which accounts for stability of crystal and molecular structure. The crystal packing of the title compound revealed that the molecules are connected to an infinite one dimensional chain along [011] direction through intermolecular hydrogen bond which further form alternative $R_2^2(14)$ and $R_4^4(20)$ supramolecular synthons. The Hirshfeld surface analysis showed that H…H (29.4%), O…H (28.7%) being the major contributors followed by C…H (16%), C…C (6.9%) and C…Cl (5.2%) interactions. The geometrical parameters calculated using DFT calculations display very good correlation with those determined by XRD method. The time dependent density functional theory (TDDFT) calculations revealed optical absorbance peak at 328 nm corresponds to the transition between the frontier molecular orbitals.

REFERENCES

[1]. C. F.Konstantina, J. H. Dimitra, E. L. Konstantinos, N. N. Demetrios, Natural and Synthetic coumarin Derivatives with Anti-Inflammatory/ Antioxidant activities, Curr.Pharm. Des., 2004, 10(30), 3813-3833.

[2]. R. K. Arora, N. Kaur, Y. Bansal, G. Bansal, Novel coumarin–benzimidazole derivatives as antioxidants and safer anti-inflammatory agents, Acta Pharm. Sin B., *2014*, 4(5), 368-375.

[3]. F. Rosskopf, J. Kraus, G. Franz, Immunological and antitumor effects of coumarin and some derivatives, Pharmazie, **1992**, 47(2), 139-142.
[4]. J. R. Hwu, R. Singha, S. C. Hong, Y. H. Chang, A. R. Das, I. Vliegen, E. D. Clercq, J. Neyts, Synthesis of new benzimidazole–coumarin conjugates as anti-hepatitis C virus agents, *Antiviral Res.*,2008, 77(2), 157-162.
[5]. A. Arshad, H. Osman, M.C. Bagley, C. K. Lam, S. Mohamad, A. S. M. Zahariluddin, Synthesis and antimicrobial properties of some new thiazolylcoumarin derivatives, *Eur. J. Med. Chem.*, 2011,46(9), 3788-3794.
[6]. H. R. Dholariya, K. S. Patel, J. C. Patel, A. K. Patel, K. D. Patel, Thermal, kinetic, spectroscopic studies and anti-microbial, anti-tuberculosis, anti-oxidant properties of clioquinol and benzo-coumarin derivatives mixed complexes with copper ion, *Med. Chem. Res.*,2013, 22(12), 5848-5860.
[7]. P. Zhou, Y. Takaishi, H. Duan, B. Chen, G. Honda, M. Itoh, Y. Takeda, O. K. Kodzhimatov, K. H. Lee, Coumarins and bicoumarin from Ferulasumbul: anti-HIV activity and inhibition of cytokine release, *Phytochemistry*, **2000**, 53(6), 689-697.
[8]. Y. Shikishima, Y. Takaishi, G. Honda, M. Ito, Y. Takeda, O. K. Kodzhimatov, O. Ashurmetov, K. H. Lee,Chemical constituents of Prangostschimganica; structure elucidation and absolute configuration of coumarin and furanocoumarin derivatives with anti-HIV activity, *Chem. Pharm. Bull.*, **2001**,49(7), 877-880.
[9]. L. Huang, X. Yuan, D. Yu, K.H. Lee, C.H. Chen, Mechanism of action and resistant profile of anti-HIV-1 coumarin derivatives, *Virology.*, **2005**, 332(2), 623-628.
[10]. Y.A. Al-Soud, H.H. Al-Sa'doni, H.A. Amajaour, K.S. Salih, M.S. Mubarakb, N.A. Al-Masoudic, Synthesis, characterization and anti-HIV and antitumor activities of new coumarin derivatives, *Z. Naturforsch. B.*, **2008**, 63(1), 83-89.
[11]. M.A. Musa, J.S. Cooper wood, M.O.F. Khan, A review of coumarin derivatives in pharmacotherapy of breast cancer, *Curr.Med.Chem.*,**2008**, 15(26), 2664-2679.
[12]. I. Kostova, Synthetic and natural coumarins as cytotoxic agents, *Curr. Med. Chem. Anticancer Agents.*, **2005**, 5(1), 29-46.
[13]. H. Chen, S. Li, Y. Yao, L. Zhou, J. Zhao, Y. Gu, X. Li, Design, synthesis, and anti-tumor activities of novel triphenylethylene–coumarin hybrids, and their interactions with Ct-DNA, *Bioorganic Med. Chem. Let.*, **2013**, 23(17), 4785-4789.
[14]. A. Lacy, R. O'kennedy,Studies on coumarins and coumarin-related compounds to determine their therapeutic role in the treatment of cancer,*Curr.Pharm.Des.*,**2004**, 10(30), 3797-3811.
[15]. R. Anil Kumar, K. M. Mahadevan, H. S. Bhojyanaik, M.V.DeepaUrs, N. K. Lokanath and S. Naveen, Synthesis, Characterization Studies of a Novel Indole Derivative: 3,3'-[(5-methylthiophen-2-yl) methanediyl]bis(1H-indole), *J. Applicable Chem.*, **2018**, 7(2), 353-360.
[16]. N. Brooker, J. Windorski, E.Bluml, Halogenated coumarin derivatives as novel seed protectants ,Commun. *Agric. Appl. Biol. Sci.*, **2008**, 73(2), 81-89.
[17]. R. Singh, B. B. Gupta, O. P. Malik, H. R. Kataria,Studies on pesticides based on coumarin. I. Antifungal activity of 6-alkyl-3-n-butyl-7-hydroxy-4-methylcoumarins, *Pest Manag. Sci.*, **1987**, 20(2), 125-130.
[18]. N. J. Van Sittert, C. P. Tuinman, Coumarin derivatives (rodenticides), *Toxicology.*, **1994**,91(1), 71-76.
[19]. K. K. Upadhyay, R. K. Mishra, A. Kumar, J. Zhao, R. Prasad, Self assembled pseudo double helix architecture and anion sensing behavior of a coumarin based ICT probe, *J. Mol. Struct.*, **2010**, 963(2), 228-233.
[20]. W. S. Chang, C. C. Lin, S. C. Chuang, H. C. Chiang, Superoxide anion scavenging effect of coumarins, *Am. J. Chin. Med.*, **1996**, 24(1), 11-17.
[21]. Y. Shiraishi, S. Sumiya, T. Hirai, Highly sensitive cyanide anion detection with a coumarin–spiropyran conjugate as a fluorescent receptor, *Chem. Comm.*, **2011**, 47(17), 4953-4955.
[22]. H. S. Jung, P. S. Kwon, J. W. Lee, J. I. Kim, C. S. Hong, J. W. Kim, S. Yan, J. Y. Lee, J. H. Lee, T. Joo, J. S. Kim,Coumarin-derived Cu^{2+}-selective fluorescence sensor: synthesis, mechanisms, and applications in living cells, *J. Am. Chem. Soc.*, **2009**, 131(5), 2008-2012.

[23]. H. Kwon, K. Lee, H.J. Kim, Coumarin–malonitrile conjugate as a fluorescence turn-on probe for biothiols and its cellular expression. *Chem. Comm*., **2001**, 47(6), 1773-1775.
[24]. K.P. Nagaraja , K.J. Pampa and N.K. Lokanath, Studies on Growth, Optical, Electrical and Dielectric Properties of Strontium and Calcium Mixed Cadmium Oxalate Crystals, *J. Applicable Chem.*, **2018**, 7(2), 457-466.
[25]. Rigaku, *Crystal Clear*, **2011**.
[26]. G. M. Sheldrick, Phase annealing in SHELX-90: direct methods for larger structures, *Acta Cryst*. A., **1990**, 46, 467-473.
[27]. G. M. Sheldrick, Crystal structure refinement with SHELXL, *Acta Cryst. C.*, **2015**, 71(1), 3-8.
[28]. A. L. Spek, PLATON, an integrated tool for the analysis of the results of a single crystal structure determination, *Acta Cryst. A*., **1990**, 46(s1), 34.
[29]. C. F. Macrae , I. J. Bruno , J. A. Chisholm , P. R. Edgington , P. McCabe , E. Pidcock , L. M. Rodriguez, R. Taylor , J. van de Streek , P.A. Wood , Mercury CSD 2.0-new features for the visualization and investigation of crystal structures, *J. Appl. Cryst*., **2008**, 41(2), 466-470.
[30]. S. K. Wolff, D.J. Grimwood, J.J. McKinnon, M.J. Turner, D. Jayatilaka, M.A. Spackman, Crystal Explorer (Version 3.0), *Uni. West. Aust*., **2012**.
[31]. S. K. Seth, Tuning the formation of MOFs by pH influence: X-ray structural variations and Hirshfeld surface analyses of with cadmium chloride, *Cryst. Eng. Comm*., **2013**, 15(9), 1772-1781.
[32]. S. K. Seth, Structural elucidation and contribution of intermolecular interactions in O- hydroxy acyl aromatics: Insights from X-ray and Hirshfeld surface analysis, *J. Mol. Struct*., **2014**, 1064, 70-75.
[33]. T. P. Jyothi, H. R. Manjunath, M. K. Ravindra, M. K. Shivanand, K. M. Mahadevan, N. K. Lokanath, S. Naveen, *J. Applicable Chem*., **2018**, 7(1), 224-233.
[34]. K. N. Chethan Prathap, R. Kayarmar, S. Naveen, M. Bhat, G. K. Nagaraja, N. K. Lokanath, Synthesis, characterization, crystal structure and hirshfeld surface analysis of (1E)-1-phenylethanone (1-Isobutyl-1H-Imidazo [4, 5-C] quinolin-4-Yl) Hydrazone. *J. Applicable Chem*., **2017**, 6(3), 400-409.
[35]. C. S. Ananda Kumar, S. Naveen, S. B. Benaka Prasad, N. S. Linge Gowda, and N. K. Lokanath, Structural Elucidation and Hirshfeld Surface Analysis of A Novel Piperazine Derivative: (4-Benzhydrylpiperazin-1-Yl)(Morpholino)Methanone, *J. Applicalbe Chem.*, **2017**, 6(2), 274-281.
[36]. C. Lee, W. Yang, R. G. Parr, Development of the Colle-Salvetti correlation-energy formula into a functional of the electron density, *Phys. Rev. B.*,**1988**, 37(2), 785.
[37]. A.D. Becke, Density-functional thermo-chemistry. I. The effect of the exchange-only gradient correction. *J. Chem. Phys*., **1992**, 96(3), 2155-2160.
[38]. P. C. Hariharan, J. A. Pople, The influence of polarization functions on molecular orbital hydrogenation energies, Theoretical Chemistry Accounts: Theory, Computation, and Modeling, Theor. *Chem. Acc.*, **1973**, 28(3), 213-222.
[39]. M. E. Casida, J. M. Seminario, RecentDevelopments and Applications of Modern Density Functional Theory, Theoretical & Computational Chemistry, vol. 4, *Elsevier*, Amsterdam, **1996**.
[40]. T. Koopmans, Über die Zuordnung von Wellenfunktionen und Eigenwertenzu den einzelnen Elektroneneines *Atoms, Physica*., **1934**, 1(1-6), 104-113.
[41]. M. J. Frisch, G. W. Trucks, H. B. Schlegel, G.E. Scuseria, M. A. Robb, J. R. Cheeseman, G. Scalmani, V. Barone, B. Mennucci, G.A. Petersson, H. Nakatsuji, M. Caricato, X. Li, H.P. Hratchian, A. F. Izmaylov, J. Bloino, G. Zheng, J. L. Sonnenberg, M. Hada, M.Ehara, K. Toyota, R. Fukuda, J. Hasegawa, M. Ishida, T. Nakajima, Y. Honda, O. Kitao, H. Nakai, T. Vreven, J. A. Montgomery Jr., J. E. Peralta, F. Ogliaro, M. Bearpark, J. J. Heyd, E. Brothers, K. N. Kudin, V. N. Staroverov, T. Keith, R. Kobayashi, J. Normand, K. Raghavachari, A. Rendell, J. C. Burant, S. S. Iyengar, J. Tomasi, M. Cossi,N. Rega, J. M. Millam, M. Klene, J. E. Knox, J. B. Cross, V. Bakken, C. Adamo, J. Jaramillo, R. Gomperts, R. E. Stratmann, O. Yazyev, A .J. Austin, R. Cammi, C. Pomelli,J. W. Ochterski, R. L. Martin, K. Morokuma, V. G. Zakrzewski, G. A. Voth, P. Salvador, J. J. Dannenberg, S. Dapprich, A. D. Daniels, O. Farkas, J. B.

Foresman, J. V. Ortiz, J.Cioslowski, D. J. Fox, Gaussian 09, Revision B.01, *Gaussian, Inc*., Wallingford, CT, **2010**.

[42]. A. Frisch, R. Dennington, T. Keith, J. Millam, A. Nielsen, A. Holder, J. Hiscocks, GaussView Version 5 User Manual, Gaussian Inc., Wallingford, CT, USA, **2009**.

[43]. K. N. ChethanPrathap, N. K. Lokanath, Synthesis, characterization, crystal structure and quantum chemical investigations of three novel coumarin-benzenesulfonohydrazide derivatives. *J. Mol. Struct*., **2018**, 1158, 26-38.